Astronomy & Astrophysics manuscript no. n113-rev4
August 11, 2016
©ESO 2016

arXiv:1409.2747v1 [astro-ph.GA] 9 Sep 2014

ASTE observations in the 345 GHz window towards the HII region N113 of the Large Magellanic Cloud

S. Paron[1,2], M. E. Ortega[1], M. Cunningham[3], P. A. Jones[3], M. Rubio[4], C. Fariña[5], and S. Komugi[6]

[1] Instituto de Astronomía y Física del Espacio (IAFE, CONICET-UBA), CC 67, Suc. 28, 1428 Buenos Aires, Argentina
e-mail: sparon@iafe.uba.ar
[2] FADU and CBC, Universidad de Buenos Aires, Argentina
[3] School of Physics, University of New South Wales, Sydney, NSW 2052, Australia
[4] Departamento de Astronomía, Universidad de Chile, Casilla 36-D, Santiago, Chile
[5] Isaac Newton Group of Telescopes, E38700, La Palma, Spain
[6] National Astronomical Observatory of Japan, 2-21-1 Osawa, Mitaka, Tokyo 181-8588

Received <date>; Accepted <date>

ABSTRACT

Aims. N113 is an HII region located in the central part of the Large Magellanic Cloud (LMC) with an associated molecular cloud very rich in molecular species. Most of the previously observed molecular lines cover the frequency range 85–270 GHz. Thus, a survey and study of lines at the 345 GHz window is required in order to have a more complete understanding of the chemistry and excitation conditions of the region.
Methods. We mapped a region of 2.′5 × 2.′5 centered at N113 using the Atacama Submillimeter Telescope Experiment in the ^{13}CO J=3–2 line with an angular and spectral resolution of 22″ and 0.11 km s^{-1}, respectively. In addition, we observed 16 molecular lines as single pointings towards its center.
Results. For the molecular cloud associated with N113, from the ^{13}CO J=3–2 map we estimate LTE and virial masses of about 1×10^4 and 4.5×10^4 M$_\odot$, respectively. Additionally, from the dust continuum emission at 500 μm we obtain a mass of gas of 7×10^3 M$_\odot$. Towards the cloud center we detected emission from: ^{12}CO, ^{13}CO, C^{18}O (3–2), HCN, HNC, HCO$^+$, C$_2$H (4–3), and CS (7–6); being the first reported detection of HCN, HNC, and C$_2$H (4–3) lines from this region. The CS (7–6) which was previously tentatively detected is confirmed in this study. By analyzing the HCN, HNC, and C$_2$H, we suggest that their emission may arise from a photodissociation region (PDR). Moreover, we suggest that the chemistry involving the C$_2$H in N113 can be similar to that in Galactic PDRs. Using the HCN J=4–3, J=3–2, and J=1–0 lines in a RADEX analysis we conclude that we are observing very high density gas, between some 10^5 and 10^7 cm^{-3}.

Key words. Galaxies: ISM – (Galaxies:) Magellanic Clouds – (ISM:) HII regions – ISM: individual objects: N113 – ISM: molecules

1. Introduction

N113 is an HII region located in the central part of the Large Magellanic Cloud (LMC). It hosts two H_2O masers, being one of them the most intense of the Magellanic Clouds (Whiteoak & Gardner 1986; Lazendic et al. 2002; Imai et al. 2013), as well as an OH maser (Brooks & Whiteoak 1997). This region is associated with a molecular cloud which is clumpy (Seale et al. 2012) and active in star formation. Indeed, three young stellar clusters, NGC 1874, NGC 1876, and NGC 1877, are related to N113 (Bica et al. 1992) and several young stellar objects (YSOs) have been found embedded in the molecular gas associated with this HII region (Sewiło et al. 2010; Seale et al. 2012; Carlson et al. 2012).

One of the main motivations of molecular observational studies towards different regions in the LMC (e.g. Johansson et al. 1994) is to study a low metallicity interstellar medium (ISM), whose physical conditions may resemble those that existed in the early Milky Way, and thus can shed light on the primeval processes of star formation. The N113 associated molecular cloud is one of the richest in the LMC and there are several studies presenting observations, with different resolutions and sensitivities, of a large number of molecular lines (Wong et al. 2006; Wang et al. 2009, and references therein). However, most of the molecular lines observed towards N113 cover the frequency range 85–270 GHz (see Chin et al. 1997; Wang et al. 2009). Only three lines were successfully observed at higher frequencies: ^{13}CO and ^{12}CO J=3–2 at 330.56 and 345.79 GHz, respectively, and HCO$^+$ J=4–3 at 356.73 GHz. Thus, a survey and study of molecular lines at the 345 GHz window (324–372 GHz) is required in order to have a more complete understanding of the chemistry and excitation conditions of the region. Therefore, we used the Atacama Submillimeter Telescope Experiment (ASTE) to map N113 in the ^{13}CO J=3–2 transition and to observe 16 molecular lines within the 345 GHz window towards its center.

2. Observations and data reduction

The molecular observations were performed between July and August 2010 with the 10 m ASTE telescope (Ezawa et al. 2004). The CATS345 GHz band receiver, a two-single band SIS receiver remotely tunable in the LO frequency range of 324-372 GHz, was used. The XF digital spectrometer was set to a bandwidth and spectral resolution of 128 MHz and 125 kHz, respec-

Send offprint requests to: S. Paron

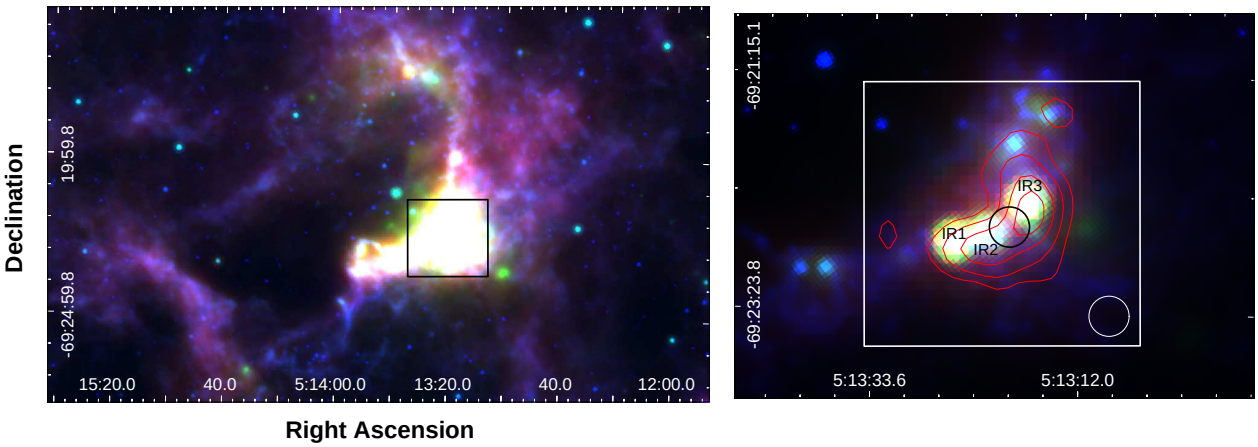

Fig. 1. Left: Three-colour image where the 8, 24, and 70 μm emission obtained from the IRAC and MIPS cameras of the Spitzer Space Telescope are presented in blue, green, and red, respectively. The black box shows the region mapped in the ^{13}CO J=3–2 line with an angular resolution of 22″. Right: Zoom-in of the mapped region (white box). The colour code is the same as in the left image but the scales are different. The red contours correspond to the ^{13}CO J=3–2 emission integrated between 230 and 245 km s^{-1} with levels of 2.5, 4.0, 6.0, and 8.0 K km s^{-1}. The FWHM beam size of the observations is included in the bottom right corner of the region. The black circle corresponds to the position where the 16 molecular lines were observed as single pointings.

Table 1. Observed molecular lines towards N113.

Molecular line	Integ. time (sec.)	Detection
^{12}CO (3–2)	200	yes
^{13}CO (3–2)	1160	yes
C^{18}O (3–2)	1160	yes
H_2D^+ (1,0–1,1)	1520	no
H_2CO (5–4)	1520	no
c-C_3H_2 (9–8)	1440	no
H_3O^+ (3,2–2,2)	480	no
HCN (4–3)	1520	yes
HNC (4–3)	800	yes
CS (7–6)	600	yes
HCO^+ (4–3)	600	yes
CH_3CN (18–17)	1280	no
CH_3CN (19–18)	1620	no(?)*
C_2H (4–3)	1620	yes
HNCO (15–14)	1280	no
DCO^+ (5–4)	1520	no

Notes. (*) see Sect. 3.2.

tively. The spectral velocity resolution was 0.11 km s^{-1} and the half-power beamwidth (HPBW) was 22″ at 345 GHz. The system temperature varied from T_{sys} = 150 to 250 K and the main beam efficiency was $\eta_{mb} \sim 0.65$.

The data were reduced with NEWSTAR[1] and the spectra processed using the XSpec software package[2]. The spectra were Hanning smoothed to improve the signal-to-noise ratio, and in some cases a boxcar smoothing was also applied. Polynomials between first and third order were used for baseline fitting.

Several molecular lines in the 345 GHz window were observed towards the center of N113 at RA = 05^{h}13^{m}19.5ß, dec. = −69 22′ 37.9″, J2000 as single pointings (black circle in Fig. 1-right). In Table 1, observed molecular lines and the integration times are listed, indicating whether the detection was positive or not. Additionally, we mapped a 2′.5 × 2′.5 region centered at RA = 05^{h}13^{m}20ß, dec. = −6922′35.5″, J2000 in the ^{13}CO J=3–2 line (white square in Fig. 1-right). This observation was performed in on-the-fly mapping mode achieving an angular sampling of 6″.

[1] Reduction software based on AIPS developed at NRAO, extended to treat single dish data with a graphical user interface (GUI).

[2] XSpec is a spectral line reduction package for astronomy which has been developed by Per Bergman at Onsala Space Observatory.

3. Results and discussion

3.1. The molecular cloud

Figure 1 (left) is a three-colour image displaying the mid/far-IR emission in the N113 area where the mapped region in the ^{13}CO J=3–2 line is indicated with a black square. Figure 1 (right) displays a zoom-in of the mapped region with a different colour scale, which allows for the identification of some point-like sources in the IR emission. The ^{13}CO J=3–2 emission integrated between 230 and 245 km s^{-1} is presented in contours showing the curved and elongated morphology of the molecular cloud in good agreement with the IR emission. The surveyed area is populated by 18 O and early-B stars (both on the main sequence and evolved), most of them with spectral types derived via UBV photometric data (Wilcots 1994). A few have spectroscopic observations as a mid-OV star (target s1 in the Wilcots study), sources BI 104 and BI 105 from Massey et al. (1995), which are B0.5V and O7V stars, and the more widely studied supergiant star, HD269217, that is of type B2[e] (e.g. Kastner et al. 2010). The main concentration of high-mass YSOs (Seale et al. 2012) and intermediate-mass YSO candidates (Carlson et al. 2012) are located in projection, along the CO emission, a configuration commonly found in massive star-forming regions (e.g. Povich et al. 2009; Book et al. 2009; Chen et al. 2010). The three conspicuous IR sources observed in Fig. 1 (right) that appear over the molecular concentration, marked as IR1, IR2, and IR3, are coincident with the compact radio continuum sources detected by Brooks & Whiteoak (1997) and with three YSOs (from southeast to northwest: 051325.09-692245.1, 051321.43-692241.5, and 051317.69-692225.0) cataloged by Seale et al. (2012) and Carlson et al. (2012). As discussed in Wong et al. (2006) these

sources could be young ionizing stars affecting the molecular gas and probably contributing to the birth of new stars.

The morphology and velocity distribution of the molecular gas related to N113 can be seen in Fig. 2, where the ^{13}CO J=3–2 emission is presented in a series of channel maps, in the range of 231-242 km s^{-1}, integrated in steps of 1 km s^{-1}. The curved and elongated molecular cloud is resolved into two clumps, one located towards the northwest and peaking at 233 km s^{-1}, the other one slightly eastwards of the center of the surveyed region, peaking at 236 km s^{-1}.

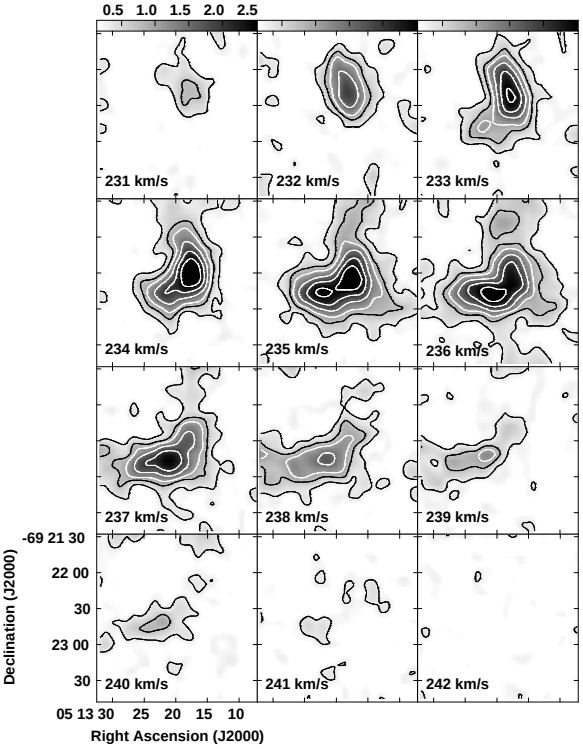

Fig. 2. Integrated velocity channel maps of the ^{13}CO J=3–2 emission every 1 km s^{-1}. The grayscale is displayed at the top of the first panel and is in K km s^{-1}, the contour levels are 0.3, 0.7, 1, 2, and 2.5 K km s^{-1}.

To derive a rough estimation of the molecular mass, we assume local thermodynamic equilibrium (LTE). We calculate the excitation temperature from:

$$T_{ex}(3 \rightarrow 2) = \frac{16.59\mathrm{K}}{\ln[1 + 16.59\mathrm{K}/(T_{\mathrm{max}}(^{12}\mathrm{CO}) + 0.036\mathrm{K})]} \quad (1)$$

where $T_{\mathrm{max}}(^{12}\mathrm{CO})$ is the ^{12}CO peak temperature towards the center of the region, obtaining $T_{ex} \sim 20$ K. We derive the ^{12}CO and ^{13}CO optical depths, τ_{12} and τ_{13}, using (e.g. Scoville et al. (1986)):

$$\frac{^{12}\mathrm{T}_{mb}}{^{13}\mathrm{T}_{mb}} = \frac{1 - exp(-\tau_{12})}{1 - exp(-\tau_{12}/X)}, \quad (2)$$

where $^{12}\mathrm{T}_{mb}$ and $^{13}\mathrm{T}_{mb}$ are the peak temperatures of the ^{12}CO and ^{13}CO J=3–2 lines at the center of the region, and $X = 50$ is the assumed isotope abundance ratio (Wang et al. 2009). The result is $\tau_{12} \sim 9.5$ and $\tau_{13} \sim 0.2$, which indicates that the ^{13}CO J=3–2 line appears optically thin. Thus, we estimate its column density from:

$$\mathrm{N} = 8.28 \times 10^{13}\, e^{\frac{15.87}{T_{ex}}} \frac{T_{ex} + 0.88}{1 - e^{\frac{-15.87}{T_{ex}}}} \frac{1}{J(T_{ex}) - J(T_{\mathrm{BG}})} \int \mathrm{T_{mb}}\, \mathrm{dv} \quad (3)$$

with

$$J(T) = \frac{h\nu/k}{exp(\frac{h\nu}{kT}) - 1}. \quad (4)$$

To obtain the molecular hydrogen column density N(H_2) we assume an abundance ratio of [H_2/^{13}CO] = 1.8×10^6, estimated by Garay et al. (2002) towards the giant molecular complex No. 37 in the LMC. Almost the same value has been obtained for N159W (Heikkilä et al. 1999), which as N113 is associated with a prominent star-forming region. Finally, the mass was derived from:

$$\mathrm{M} = \mu\, m_{\mathrm{H}} \sum_i \left[D^2\, \Omega_i\, \mathrm{N}_i(\mathrm{H_2})\right], \quad (5)$$

where Ω is the solid angle subtended by the beam size, D is the distance (50 kpc), m_{H} is the hydrogen mass, and μ is the mean molecular weight, assumed to be 2.8 by taking into account a relative helium abundance of 25 %. The summation was performed over all beam positions belonging to the molecular structure displayed in contours in Fig. 1 (right panel). The obtained mass is about 1×10^4 M$_\odot$, which is somewhat lower than the 8.2×10^4 M$_\odot$ estimated by Wong et al. (2006) from the ^{12}CO J=1–0 line using a standard Galactic CO to H_2 conversion factor ($\mathrm{N_{H_2}/I_{CO}} = 2.0 \times 10^{20}$ cm^{-2} (K km s^{-1})$^{-1}$). This discrepancy may be due to that the ^{13}CO J=3–2 and the ^{12}CO J=1–0 map different extensions of the molecular cloud, and/or suggests that the Galactic CO to H_2 conversion factor used by Wong et al. is not appropriate for N113.

From the average of the ^{13}CO J=3–2 emission towards the molecular structure we obtain an averaged spectrum with Δv = 5.3 km s^{-1}. Roughly approximating the molecular cloud with a spherical shape of radius 35″ (R = 8.8 pc) and considering a density profile of $\rho \propto r^{-1}$ we estimate the virial mass from (MacLaren et al. 1988):

$$\frac{M_{\mathrm{vir}}}{\mathrm{M}_\odot} = 190 \left(\frac{R}{\mathrm{pc}}\right) \left(\frac{\Delta \mathrm{v}}{\mathrm{km\ s^{-1}}}\right)^2, \quad (6)$$

which gives $\sim 4.5 \times 10^4$ M$_\odot$.

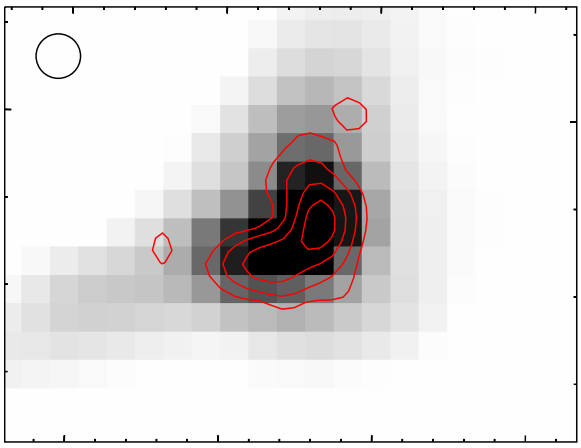

Fig. 3. 500 μm emission obtained from SPIRE in the Herschel Space Observatory with the same ^{13}CO J=3–2 contours as shown in Fig. 1 (right). The FWHM beam size of the molecular observations is included in the top left corner. The angular resolution of the SPIRE image is about 36″.

Additionally, we estimate the mass of gas of the N113 cloud from the continuum emission at the far-infrared regime arising

Table 2. Line parameters for the molecular lines presented in Figs. 4 and 5.

Molecular line	$\int T_{mb} dv$ (K km s^{-1})	T_{mb} peak (K)	v_{LSR} (km s^{-1})	Δv (FWHM) (km s^{-1})
^{12}CO (3–2)	66.20±2.20	9.90±0.30	235.84±0.10	6.25±0.20
^{13}CO (3–2)	9.52±1.50	1.73±0.32	236.58±0.47	5.23±1.10
C^{18}O (3–2)	0.35±0.10	0.05±0.02	235.68±0.55	4.73±1.70
CS (7–6)	0.54±0.18	0.08±0.02	235.15±0.80	5.75±1.20
HCO$^+$ (4–3)	3.40±0.20	0.47±0.10	233.90±0.95	7.15±1.50
HCN (4–3)	0.70±0.15	0.09±0.02	234.28±0.75	8.22±1.50
HNC (4–3)	0.35±0.10	0.08±0.02	234.87±0.70	3.85±1.00

from the dust. To do so we obtain the integrated flux of the continuum emission at 500 μm using the calibrated level 2 PLW SPIRE image extracted from the Herschel Data Archive (ObsID:1342202224). Figure 3 displays the 500 μm emission with contours of the ^{13}CO J=3–2, showing that both emissions are very similar in morphology and size. From the radiative transfer equation and assuming an optically thin medium we can estimate the gas mass in the cloud as:

$$M_{gas} = \frac{S_\lambda D^2}{\kappa_d(\lambda) x_d B_\lambda(T_d)}, \quad (7)$$

where S_λ, D, $\kappa_d(\lambda)$, x_d, and $B_\lambda(T_d)$ are the integrated flux at 500 μm, the distance, the dust absorption coefficient, the dust-to-gas mass ratio, and the Planck's law at the T_d dust temperature, respectively. Considering the obtained integrated flux at 500 μm of about 50 Jy, a distance of 50 kpc, $\kappa_d(500\mu m) = 1.14$ for the LMC (Weingartner & Draine 2001), a T_d of about 24 K and $x_d = 1.7 \times 10^{-3}$ (Verdugo et al. 2011) we derive a mass of gas of about 7×10^3 M$_\odot$. This value is almost two orders of magnitude lower than the mass estimated by Wang et al. (2009) from the 1.2 mm dust continuum. The M_{vir}/M_{gas} ratio is larger than unity, as found in several clouds in N11 (Herrera et al. 2013), a bright HII region in the LMC hosting several star clusters.

3.2. Molecular lines

In Figs. 4 and 5 we present the spectra of the molecular lines successfully observed towards the position indicated with a black circle in Fig. 1 (right). Figure 4 shows the CO isotopologues, and Fig. 5, the emission of the detected rarer lines. The line parameters given in Table 2 were obtained from single-component Gaussian fits. All the spectra have signals well above the 3σ, except the C^{18}O J=3–2 line, for which the signal is evident but the noise is high. It is important to note that the HNC and HCN lines are detected for the first time towards N113 in the J=4–3 transition. On the other side, the CS J=7–6 line was tentatively detected by Wang et al. (2009) and in this study we confirm its detection. Our CS central velocity and Δv are in agreement, within the errors, with the previous tentative detection. Taking into account that the critical density of the HCN J=4–3 line is about 10^8 cm^{-3} (Takakuwa et al. 2007), we conclude that we are observing a high density molecular clump, which is in agreement with the conspicuity of the CS J=7–6 line, also a tracer of high density gas.

Figure 6 shows the obtained spectrum in the frequency range 349.30 – 349.43 GHz, which is populated by several lines and fine structure components of C_2H and CH_3CN. The frequencies where molecular emission lines are expected according to the NIST data base[3], are indicated in the figure and listed in Table 3. In the spectrum presented in Fig. 6 two peaks can be distinguished, likely due to the C_2H (4–3) fine structure transitions. The peak centred around 349.342 GHz is composed by two C_2H blended hyperfine lines and probably by one line of the CH_3CN 19–18 transition. The other peak, centred around 349.403 GHz, is also composed by two C_2H blended hyperfine lines. Chin et al. (1997) and Wang et al. (2009) have reported the

[3] http://www.nist.gov/pml/data/micro/index.cfm

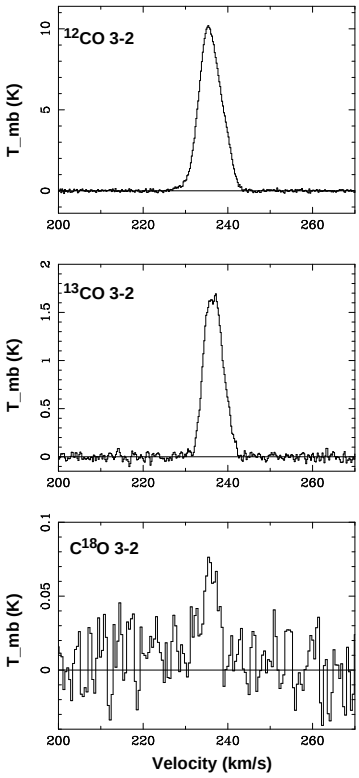

Fig. 4. CO isotopologues obtained towards the center of N113. The rms noise levels of each spectrum are: 80, 35, and 30 mK, respectively, and the displayed channel spacings are about 0.2 km s^{-1} for the ^{12}CO and ^{13}CO, and 0.4 km s^{-1} for the C^{18}O.

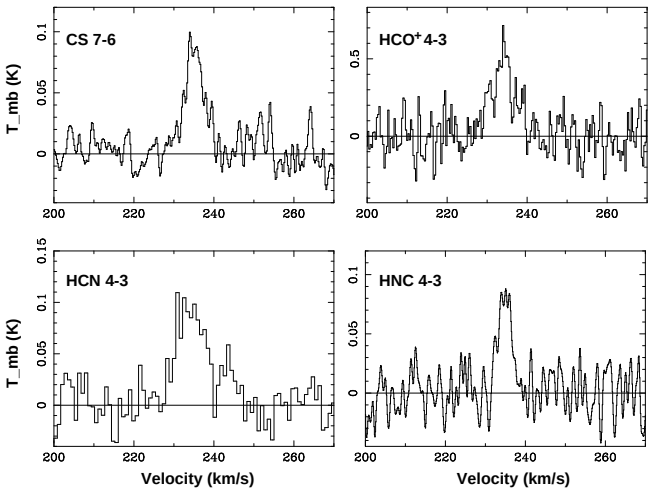

Fig. 5. Spectra of CS J=7–6 and HCO$^+$, HCN, and HNC J=4–3 obtained towards the center of N113. The rms noise levels of each spectrum are: 14, 90, 20, and 13 mK, respectively, and the displayed channel spacings are about 0.2 km s^{-1} for the CS, HCO$^+$, and HNC, and 1.2 km s^{-1} for the HCN.

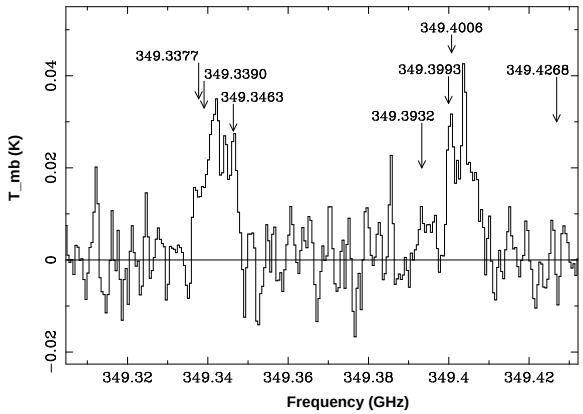

Fig. 6. Spectrum in the frequency range 349.30 – 349.43 GHz. The arrows indicate the frequencies where molecular emission lines are expected, according to the NIST data base (see Table 3). The rms noise is about 6 mK and the displayed channel spacing is about 0.5 MHz.

Table 3. Molecular lines within the 349.30 – 349.43 GHz range (see spectrum in Fig. 6).

Frequency (GHz)	Molecule	Transition (quantum numbers)
349.3377	C_2H	4–3 *J*=9/2-7/2 F=5-4
349.3390	C_2H	4–3 *J*=9/2-7/2 F=4-3
349.3463	CH_3CN	19(4)–18(4)
349.3932	CH_3CN	19(3)–18(3)
349.3993	C_2H	4–3 *J*=7/2-5/2 F=4-3
349.4006	C_2H	4–3 *J*=7/2-5/2 F=3-2
349.4268	CH_3CN	19(2)–18(2)

detection of C_2H (1–0) *J*=3/2–1/2 F=2-1 and 1-0 lines towards N113 and in this study we are presenting the first detection of C_2H (4–3) towards this region. Regarding the CH_3CN 19(4)–18(4) line, probably blended in the peak centred around 349.345 GHz, it is not possible to confirm its detection in our observations. Besides, the non-detection of the CH_3CN 18–17 line, a lower transition, also suggests a non-detection for the J=19–18 transition.

Beuther et al. (2008) observed C_2H (4–3) towards a Galactic sample of star forming regions in different evolutionary stages, including infrared dust clouds (IRDCs), high mass protostellar objects (HMPOs), and ultracompact HII regions (UCHIIs). They found that the C_2H lines are detected independently of the evolutionary stage of the sources, but the UCHIIs regions exhibit line widths in both C_2H (4-3) main peaks significantly broader than the others objects (on average about 5.5 km s^{-1}). Assuming that the peaks in the spectrum of Fig. 6 are due exclusively to emission of C_2H, and converting the frequency into velocity, we measure the FWHM of both peaks as 6.8 and 6.4 km s^{-1}, respectively, indicating that both are broad lines as those measured by Beuther et al. (2008) towards UCHIIs. This result is in agreement with the presence of the compact radio continuum sources detected by Brooks & Whiteoak (1997) in N113. Besides, the position where the molecular lines were observed in this study lies between the two most intense continuum sources in the study of Wong et al. (2006) (sources 2 and 3; IR2 and IR3 in Fig. 1-right). The authors have estimated that the equivalent to one or two O6 stars is needed to produce the measured fluxes in the radio continuum (at 24 and 86 GHz) towards source 2, which, as discussed in their study, should be young ionizing stars affecting the molecular gas. Indeed, the C_2H can be formed and/or replenished after destruction in earlier stages, in PDRs, through $C_2H_2 + h\nu \rightarrow C_2H + H$. The neutral-neutral reaction $CH_2 + C \rightarrow C_2H + H$ can also produce C_2H, where the precursor carbon atom is formed through the photodissociation of CO (Miettinen 2014, and references therein). Therefore, we suggest that the chemistry involving this radical in N113 can be similar to that proceeding in Galactic PDRs.

Table 4. Integrated intensity ratios towards N113.

Ratio	this work	Chin et al. (1997) (all J=1–0)	Wang et al. (2009)
$\frac{^{12}CO}{^{13}CO}$	6.9 ± 1.1	7.28 ± 0.70	4.50 ± 0.16 (J=3–2)
$\frac{^{13}CO}{C^{18}O}$	27.0 ± 8.8*	35.8 ± 3.1	39.8 ± 2.7 (J=1–0)
$\frac{HCO^+}{HCN}$	4.8 ± 1.1	1.34 ± 0.06	1.47 ± 0.10 (J=1–0) 2.15 ± 0.47 (J=3–2)
$\frac{HCN}{HNC}$	2.0 ± 0.7	2.8 ± 0.2	2.6 ± 0.2 (J=1–0)
$\frac{HNC}{HCO^+}$	0.10 ± 0.03	0.26 ± 0.01	0.26 ± 0.01 (J=1–0)

Notes. (*) Tentatively ratio due to the high noise in the $C^{18}O$ spectrum.

In Table 4 the observed integrated intensity ratios are listed for the lines presented in Table 2, together with a comparison with ratios obtained using the J=1–0 transitions from Chin et al. (1997) and from Wang et al. (2009) for the transitions indicated in the Table. Our results are in good agreement with the ratios obtained from lower transitions, except for the HCO^+/HCN and HNC/HCO^+ ratios. The HCO^+/HCN ratio is larger than unity as was found in several Magellanic giant molecular clouds, suggesting that the ion abundance is higher than in Galactic clouds, where this ratio was found to be lower than unity (Stacey et al. 1991; Chin et al. 1997). This must be due to higher UV fields in the Magellanic environments. Additionally, the low nitrogen abundance in the LMC (e.g. Hunter et al. 2007; Bekki & Tsujimoto 2010) can also contribute in the increment of the HCO^+/HCN ratio. Furthermore, it seems that the HCO^+/HCN ratio increases for increasing rotational transitions, which suggests that the physical conditions in N113 may favour the excitation of the HCO^+ higher transitions more efficiently than those of HCN. If the HCO^+ and HCN emission occur in the same region, the increment in the HCO^+/HCN ratio with the rotational transitions may reflect different critical densities, with HCN being selectively de-excited at higher transitions. Indeed, even though the E_u/k_B factor is similar in both molecular species, their critical densities vary between different J_u–J_l transitions (n_{crit}(HCN)/n_{crit}(HCO^+) ~ 5–7 for J = 1–0, 3–2, and 4–3; Papadopoulos 2007). Similar cases of this HCO^+/HCN ratio behaviour were found towards the Galactic NGC 1333-IRAS 2A outflow (Jørgensen et al. 2004) and towards the nuclear region of M82 (Seaquist & Frayer 2000). Regarding the HCN/HNC ratio, it is larger than unity in the J=4–3 line, as is the case for the lower transitions, supporting the prediction by Chin et al. (1997) that the ratio would be large in warm gas subject to strong UV heating, but approaches unity in cloud cores. Also Wang et al. (2009) point out that the HCN/HNC ratio larger than unity may indicate a PDR scenario, which is in agreement with the C_2H chemistry discussed above.

Using the derived HCN J=4–3 parameters listed in Table 2 and the HCN J=3–2 and J=1–0 parameters presented in Wang et al. (2009) we perform a non-LTE study of this

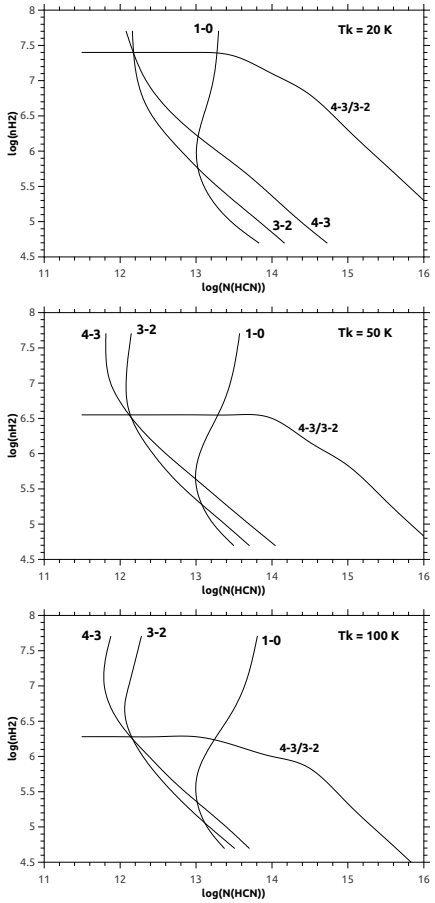

Fig. 7. Radex calculations for the HCN J=4–3 and 3–2 lines for kinetic temperatures of 20, 50, and 100 K. The results for HCN J=1–0 are included for comparison with Wang et al. (2009).

molecular species using RADEX (van der Tak et al. 2007). The RADEX model uses the mean escape probability approximation for the radiative transfer equation. As done by Wang et al. (2009), we correct for beam dilution by calculating $T'_{mb} = T_{mb}/\eta_{bf}$, with $\eta_{bf} = \theta_s^2/(\theta_s^2 + \theta_b^2)$, where θ_b and θ_s are the beam and the source size. Following Wang et al., a source size of 40″ was assumed. Then we run the RADEX code using the measured Δv to fit T'_{mb} for each transition. Figure 7 shows the RADEX calculations for the HCN, displaying the expected H_2 density and N(HCN) pairs that correspond to a given T'_{mb} and 4–3/3–2 intensity ratio. The calculations were made for kinetic temperatures of 20, 50, and 100 K, as done in previous studies (see Wang et al. 2009 and references therein). The obtained results from the J=4–3 and J=3–2 lines are presented in Table 5. The results from the J=3–2 and J=1–0 lines are similar to those obtained by Wang et al. (2009), that is a density of several 10^5 cm^{-3}, and N(HCN) of about 1×10^{13} cm^{-2}. Thus we conclude that the HCN column density ranges from 1.4×10^{12} to about 1×10^{13} cm^{-2}, and the density varies from some 10^5 to a few 10^7 cm^{-3}. Our results confirm that the HCN emission emanates from a very high density region in N113. The density of this region ranges between the HCO^+ and HCN J=4–3 critical densities, which can explain the dependency of the HCO^+/HCN ratio on the rotational transitions discussed above.

Table 5. Radex results from the HCN 4–3 and 3–2 lines.

T_k (K)	n_{H_2} (cm^{-3})	N(HCN) (cm^{-2})	τ_{4-3}	τ_{3-2}
20	2.51×10^7	1.47×10^{12}	0.014	0.018
50	3.23×10^6	1.38×10^{12}	0.014	0.019
100	1.82×10^6	1.43×10^{12}	0.014	0.020

4. Summary

N113 is an HII region located in the central part of the Large Magellanic Cloud with an associated molecular cloud very rich in molecular species. At present, most of the observed molecular lines cover the frequency range 85–270 GHz, requiring a survey at higher frequencies in the 345 GHz window in order to have a more complete understanding of the chemistry and excitation conditions of the region. To perform that, we mapped a region of 2.′5 × 2.′5 centered at N113 using the Atacama Submillimeter Telescope Experiment in the ^{13}CO J=3–2 line with an angular and spectral resolution of 22″ and 0.11 km s^{-1}, respectively, and observed 16 molecular lines as single pointings towards its center. The main results can be summarized as follows:

(1) The N113 associated molecular cloud mapped in the ^{13}CO J=3–2 line shows a curved and elongated morphology in good agreement with the IR emission. From this line we estimated LTE and virial masses for the molecular cloud of about 1×10^4 and 4.5×10^4 $M_\odot$, respectively. Additionally, from the dust continuum emission at 500 μm we obtained a mass of gas of 7×10^3 $M_\odot$.

(2) Towards the center of the N113 molecular cloud we detected emission from: ^{12}CO, ^{13}CO, C^{18}O (3–2), HCN, HNC, HCO^+, C_2H (4–3), and CS (7–6), being the first reported detection of HCN, HNC, and C_2H in the J=4–3 line from this region. CS (7–6), which was previously tentatively detected, was confirmed in this study. The detection of HCN (4–3) and CS (7–6) reveals a very high density region .

(3) The observed C_2H (4–3) presents two peaks due to its fine structure transitions. We suggest that the chemistry involving the C_2H in N113 is similar to that in Galactic PDRs.

(4) We found that the HCN/HNC ratio is larger than unity in the J=4–3 line, as is the case for lower transitions, supporting the prediction that this ratio would be large in warm gas subject to strong UV heating, indicating a PDR scenario, which is in agreement with our finding of broad C_2H lines. Additionally, we found that HCO^+/HCN ratio increases with increasing rotational transitions, showing different critical densities for both molecular species.

(5) Using the parameters derived from our HCN J=4–3 observation and previous results from HCN J=3–2 and J=1–0 we performed a non-LTE study of this molecule. Our results confirm that the HCN emission emanates from a very high density region in N113, with densities ranging between some 10^5 and 10^7 cm^{-3}.

Acknowledgements. We thank the anonymous referee for her/his helpful comments and corrections. The ASTE project is led by Nobeyama Radio Observatory (NRO), a branch of National Astronomical Observatory of Japan (NAOJ), in collaboration with University of Chile, and Japanese institutes including University of Tokyo, Nagoya University, Osaka Prefecture University, Ibaraki University, Hokkaido University, and the Joetsu University of Education. S.P. and M.O. are members of the *Carrera del investigador científico* of CONICET, Argentina. This work was partially supported by grants awarded by CONICET, ANPCYT and UBA (UBACyT) from Argentina. M.R. wishes to acknowledge support from CONICYT through FONDECYT grant No 1140839.

References

Bekki, K. & Tsujimoto, T. 2010, ApJ, 721, 1515
Beuther, H., Semenov, D., Henning, T., & Linz, H. 2008, ApJ, 675, L33
Bica, E., Claria, J. J., & Dottori, H. 1992, AJ, 103, 1859
Book, L. G., Chu, Y.-H., Gruendl, R. A., & Fukui, Y. 2009, AJ, 137, 3599
Brooks, K. J. & Whiteoak, J. B. 1997, MNRAS, 291, 395
Carlson, L. R., Sewiło, M., Meixner, M., Romita, K. A., & Lawton, B. 2012, A&A, 542, A66
Chen, C.-H. R., Indebetouw, R., Chu, Y.-H., et al. 2010, ApJ, 721, 1206
Chin, Y.-N., Henkel, C., Whiteoak, J. B., et al. 1997, A&A, 317, 548
Ezawa, H., Kawabe, R., Kohno, K., & Yamamoto, S. 2004, in Presented at the Society of Photo-Optical Instrumentation Engineers (SPIE) Conference, Vol. 5489, Society of Photo-Optical Instrumentation Engineers (SPIE) Conference Series, ed. J. M. Oschmann, Jr., 763–772
Garay, G., Johansson, L., Nyman, L.-Å., et al. 2002, A&A, 389, 977
Heikkilä, A., Johansson, L., & Olofsson, H. 1999, A&A, 344, 817
Herrera, C. N., Rubio, M., Bolatto, A. D., et al. 2013, A&A, 554, A91
Hunter, I., Dufton, P. L., Smartt, S. J., et al. 2007, A&A, 466, 277
Imai, H., Katayama, Y., Ellingsen, S. P., & Hagiwara, Y. 2013, MNRAS, 432, L16
Johansson, L. E. B., Olofsson, H., Hjalmarson, A., Gredel, R., & Black, J. H. 1994, A&A, 291, 89
Jørgensen, J. K., Hogerheijde, M. R., Blake, G. A., et al. 2004, A&A, 415, 1021
Kastner, J. H., Buchanan, C., Sahai, R., Forrest, W. J., & Sargent, B. A. 2010, AJ, 139, 1993
Lazendic, J. S., Whiteoak, J. B., Klamer, I., Harbison, P. D., & Kuiper, T. B. H. 2002, MNRAS, 331, 969
MacLaren, I., Richardson, K. M., & Wolfendale, A. W. 1988, ApJ, 333, 821
Massey, P., Lang, C. C., Degioia-Eastwood, K., & Garmany, C. D. 1995, ApJ, 438, 188
Miettinen, O. 2014, A&A, 562, A3
Papadopoulos, P. P. 2007, ApJ, 656, 792
Povich, M. S., Churchwell, E., Bieging, J. H., et al. 2009, ApJ, 696, 1278
Scoville, N. Z., Sargent, A. I., Sanders, D. B., et al. 1986, ApJ, 303, 416
Seale, J. P., Looney, L. W., Wong, T., et al. 2012, ApJ, 751, 42
Seaquist, E. R. & Frayer, D. T. 2000, ApJ, 540, 765
Sewiło, M., Indebetouw, R., Carlson, L. R., et al. 2010, A&A, 518, L73
Stacey, G. J., Geis, N., Genzel, R., et al. 1991, ApJ, 373, 423
Takakuwa, S., Ohashi, N., Bourke, T. L., et al. 2007, ApJ, 662, 431
van der Tak, F. F. S., Black, J. H., Schöier, F. L., Jansen, D. J., & van Dishoeck, E. F. 2007, A&A, 468, 627
Verdugo, C., Rubio, M., & Bolatto, A. 2011, Boletin de la Asociacion Argentina de Astronomia, 54, 247
Wang, M., Chin, Y.-N., Henkel, C., Whiteoak, J. B., & Cunningham, M. 2009, ApJ, 690, 580
Weingartner, J. C. & Draine, B. T. 2001, ApJ, 548, 296
Whiteoak, J. B. & Gardner, F. F. 1986, MNRAS, 222, 513
Wilcots, E. M. 1994, AJ, 108, 1674
Wong, T., Whiteoak, J. B., Ott, J., Chin, Y.-n., & Cunningham, M. R. 2006, ApJ, 649, 224